Egyptian Journal of Soil Science
http://ejss.journals.ekb.eg/

Environmental and Spatial Assessment of Urban Heat Islands in Qalyubia Governorate, Egypt

Mahmoud S. Ibrahim[1], Maie I. El-Gammal[1], Adel Shalaby[2], Ahmed M. El-Zeiny[2] and Neven G. Rostom[2*]

[1]*Environmental Science Department, Faculty of Science, New Damietta, Damietta University, Egypt*

[2]*Environmental Studies and Land Use Division, National Authority for Remote Sensing and Space Sciences (NARSS), Cairo, Egypt*

The present study is the first attempt to map Urban Heat Islands (UHIs) and assess the associated environmental characteristics in Qalyubia Governorate using remote sensing and GIS integrated with a field survey. A calibrated Landsat Operational Land Imager (OLI) acquired on July 22, 2018 was processed to calculate Land Surface Temperature (LST) and UHIs as well as to evaluate the environmental conditions through calculating the Land Use Land Cover (LULC) and the spectral retrieved indices. The investigated indices include Normalized Difference Built-Up Index (NDBI), Normalized Difference Vegetation Index (NDVI), Modified Normalized Difference Water Index (MNDWI), Normalized Difference Salinity Index (NDSI) and Normalized Difference Moisture Index (NDMI). Likewise, multispectral algorithm model was applied on the landsat calibrated image for mapping Particulate Matter of diameters lower than 10 micrometer (PM_{10}) and characterizing its levels in the UHIs. The results demonstrated that the mean LST of each LULC class in Qalyubia Governorate followed this order; bare lands > urban > vegetation > water bodies. Most of bare land and built-up areas exist as heat island regions. The total area of UHI_s was 397.5 km^2; 119.8 km^2 as bare land (30.2%), 201.2 km^2 as built-up (50.6%), 0.2 km^2 as water (0.05%) and 76.3 km^2 as vegetation (19.2%). Low mean values of NDVI and MNDWI were observed in association with UHIs regions which confirmed the positive impact of green cover and water bodies in eliminating UHIs phenomena. On other hand, NDBI showed high mean level in UHIs comparing to its levels in the study area. The average value of PM_{10} over UHI (94.26 µg/m^3) was more than that in the study area (81.07 µg/m^3). It can be concluded that the decrease in green spaces and water bodies as well as the increase in urban density lead to increasing the intensity and widespread of UHIs phenomenon. Therefore, the study recommends the necessity to consider results of the present study for urban designers, planners, and architects in designing and planning urban communities.

Keywords: Urban heat island, Landsat images, Environmental characterization, Land surface temperature

Introduction

Urban encroachment has some negative impacts on the global environment, including air quality, temperature increases and landscape change. It also leads to agricultural land area decrease and loss of biodiversity (Santamouris et al., 2001, Shalaby and Moghanm, 2015). The elevation of surface air temperature is considered as the most obvious change in the climate (Jones et al., 1986) which causes an increase in the death rate in humans (Hajat et al., 2010) as at high temperatures the central nervous thermoregulatory system of the human body fails to operate (Jay and Kenny, 2010). In general, in urban environments, the temperature is observed to be higher in comparison to that at

*Corresponding author: neven.gamal@narss.sci.eg
DOI: 10.21608/ejss.2019.10917.1258
Received 20/3/2019; Accepted 15/5/2019
©2019 National Information and Documentation Centre (NIDOC)

nearby rural areas. This phenomenon is called the urban heat island (UHI) effect. The UHI represents any urban areas radiating higher temperatures than the warmest temperatures associated with tree canopy (Arya, 2001).

The reasons for UHI are different, including characteristic components and human variables, where the main cause is the land use change. Moreover, the factors such as, urban encroachment, heat discharge from anthropogenic warmth source, atmospheric pollution, geographic location, and climate additionally influence the UHI (Nakayama and Hashimoto, 2011).

Qalyubia Governorate is characterized by a high population density filled with high structures and industrial facilities and has an absence of open spaces in urban territories, along these lines, therefore the urban zones suffer from a serious UHI effects. The traditional strategy for studying UHI relies on meteorology data derived from urban and weather stations. It is hard to get abundant meteorology data and to gain surface meteorology data, besides specked meteorology information (Tomlinson et al., 2012). The thermal band of the satellite images, including the Landsat Thematic Mapper (TM) images, Landsat OLI, Advanced Space borne Thermal Emission and Reflection Radiometer (ASTER) and Moderate Resolution Imaging Spectroradiometer (MODIS); can be transformed to LST to study the UHI. Rao, 1972 was the first to recommend that remote sensing is useful for studying the UHI and producing a graph for land surface thermal distribution by the thermal infrared data from satellite images. After that, satellite images have been generally used to study the LST and UHI (Amorim and Dubreuil, 2017).

Landsat imageries have been also used intensively in mapping LULC and in detection of changes (Shen et al., 2011). Therefore, studying LULCC has been considered an important research in the spatial analysis of remote sensing (RS) since the 1970s (Lo & Shipman, 1990 and Shalaby & Tateishi, 2007). Arveti et al. (2016) used RS geospatial techniques for monitoring LULC in Tirupati Area at South India. Liping et al. (2018) used remote sensing and GIS techniques for predicting and evaluating and LULCC in a hilly area, Jiangle, China.

Moreover, Teka et al. (2018) studied LULC using pastoralists' perceptions and Landsat images in assessing land cover temporal changes at Borana lands, southern Ethiopia. Furthermore, from the mid of the 1990s, various spectral indices as NDVI, NDBI, MNDWI, NDSI NDMI could be used for accurate and fast classification from satellite images (Tucker, 1979, Weigand & Richardson, 1990, Masek et al., 2000, Ji et al., 2009, Anim et al., 2013 and Elbeih & El-Zeiny, 2018).

The quick urbanization process, the persistent development, the industry development and the expanded transportation lead to a more serious air pollution issue. The World Health Organization (WHO) stated that urban air pollution causes death of 800,000 peoples and decrease of life expectancy of 4.6 million people in the world every year. However, air pollutants can be interpolated based on data from monitoring stations to measure the pollution level which are very costly (Nadzri et al., 2010). International studies confirm that the usage of satellite imagery can monitor air pollution. The application of remote sensing technique in the air pollution field should be addressed first at the macro level to support decision makers in planning regions and the development of industrial zones and urban areas (Nadzri et al., 2010).

Both short term and long term exposure to ambient levels of PM_{10} are consistently associated with respiratory and cardiovascular illness and mortality as well as other ill-health effects. The associations are believed to be casual. It is not currently possible to discern a threshold concentration below which there are no effects on the whole population's health. The PM_{10} roughly equates to the mass of particles less than 10 μm in diameter that are likely to be inhaled into the thoracic region of the respiratory tract (Caldero et al., 2004). Therefore, Satellite imagery is used to monitor air quality in urban areas and this is a cost effective methodology. Therefore, in this study the ability of predicting PM_{10} in atmosphere has obtained using the Landsat 8 images.

The aim of this study was to assess and map LST and UHIs in Qalyubia Governorate using the thermal bands of a calibrated multispectral image. The land characteristics of UHI regions would be assessed through four spectral indices and LULC retrieved from the multispectral bands of the calibrated image. The spatial distribution of PM_{10} in these regions would also be assessed to highlight the relationship between UHIs and air quality.

Materials and Methods

Study area and field survey

Qalyubia Governorate is located on the eastern side of the River Nile, near the delta head between

30˚ 06′ 11″ to 30˚ 36′ 36″ North and 31˚ 03′ 20″ to 31˚ 35′ 32″ East. Its boundary from the south is both Cairo and Giza Governorates, from the north is Dakahlia and Gharbia Governorates, from the east is El-Sharkia Governorate and from the west is El-Monofia Governorate as shown in Fig. 1. The governorate is characterized by a specific location as it is considered the meeting point of the main transport lines between northern governorates. The total area is estimated to be 1001.09 km^2, where the cultivated area is 810 km^2; representing 81% of its total coverage. The common activity in the governorate is mostly agriculture, in addition to the existence of some industrial parks.

Qalyubia climate is characterized by an extreme aridity, long hot rainless summer, short rainy mild winter, high evaporation and low relative humidity. Evaporation varies in different months of the year. It ranges between 94 mm/day in winter and 278 mm/day in summer. Relative humidity varies between 55.5% in June and 72.1% in August. Wind velocity ranges from 2.7 km/h in August to 5.8 km/h in March (Bahteim Meteorological Station, 2009).

A field survey was conducted during the period from 18th to 19th july 2018 to assess and explore the study area characteristics such as agricultural land properties and industrial activities. During the field survey, a total number of 30 different sites covering most parts of the study area were visited and the dominant characteristics at each site were reported for assessment purposes.

Satellite sensors acquisition and preprocessing

In the current study, Landsat 8 (July 22, 2018) OLI was freely downloaded in the scene (176 and 39). Two preprocessing techniques were applied on the accessed image; atmospheric correction and radiometric calibration (dark object subtraction (DOS)) using ENVI 5.1 software. The DOS technique was used and applied on the radiometrically calibrated image to eliminate atmospheric scattering effect. The calibrated image is finally cropped to map the study area.

LULC and Spectral indices

The multispectral bands of the calibrated image are processed to produce LULC, NDVI, MNDWI, NDSI, NDMI and NDBI to identify the land features of the study area. However, the thermal bands were processed to map LST and UHIs in the study area. By using the supervised classification (Maximum Likelihood Classifier); an up-to-date LULC map is produced for the Landsat calibrated image. It is carried out to define human activities and natural resources dominating the study area. The resultant LULC categories are: urban area, desert, water bodies and vegetation (Nile River and Canals). To calculate the accuracy, the image spectral statistics are computed using

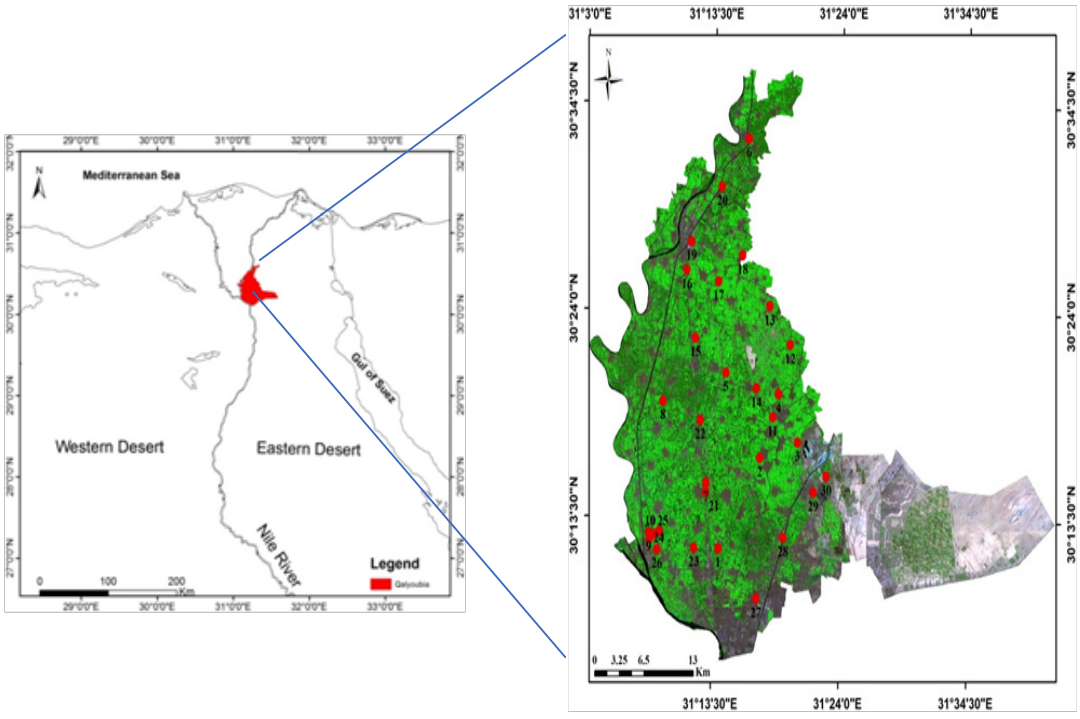

Fig. 1. Location map of the study areashowing the field surveyed sites

ENVI 5.1 software while all pixels -in the image- are correctly calibrated (Abdel-Hamid, 2010). Overall accuracy was finally calculated based on the field verification points to assess the accuracy of the produced LULC map.

Modified Normalized Difference Water Index (MNDWI)

Xu (2006) proposed the MNDWI for extracting waterlogged areas that was calculated as follows:

$$MNDWI = \frac{(Green-SWIR)}{Green+SWIR} \quad (1)$$

where SWIR is the short-wave infrared band and Green is a green band. MNDWI ranges from −1.0 to +1.0 where +0.1 to +0.4 is the green vegetation common range.

Normalized Difference Built-Up Index (NDBI)

The built-up land was produced using the NDBI of Zha et al. (2003) as follows:

$$NDBI = \frac{SWIR-NIR}{SWIR+NIR} \quad (2)$$

where, NIR is a near infrared band.

Normalized Difference Salinity Index (NDSI)

Soil salinity indices are mostly used to distinguish salt mineral in soils based on different responses of salty soils to different spectral bands. NDSI is the reverse of the NDVI (Tucker, 1979; Jabbar and Xiaoling, 2008). The algorithm is shown in Eq. (3) as follows:

$$NDSI = \frac{Red-NIR}{Red+NIR} \quad (3)$$

Normalized Difference Vegetation Index (NDVI)

The NDVI is used for change detection analysis in many studies (de Boer, 2000; Huang and Siegert, 2006 and Ahl et al., 2006). The NDVI was calculated using the Eq. (4) as follows.

$$NDVI = \frac{NIR-Red}{NIR+Red} \quad (4)$$

The value of this index ranges from −1.0 to 1.0 while 0.2-0.8 is the common range for green vegetation. Higher value of NDVI refers to the presence of healthy vegetation in the area while its lower value refers to sparse vegetation.

Normalized Difference Moisture Index (NDMI)

The NDMI derived from Landsat spectral bands near infrared (NIR) and mid infrared (MIR) (Gao, 1996) and calculated using eq. (5) as follows:

$$NDMI = \frac{NIR-MIR}{NIR+MIR} \quad (5)$$

This index contrasts NIR, that is sensitive to the reflectance of leaf chlorophyll content to MIR, that is sensitive to the leaf moisture absorbance.

Land Surface Temperature (LST) and mapping Urban Heat Islands (UHIs)

Deriving LST from Landsat thermal band

The different satellite sensors get temperature data and store the information as a digital number (DN) with a range between 0 and 255. The first step is the transforming DNs to radiance values and then converts it into degrees Kelvin (Coll et al., 2010).

Conversion of digital number to spectral radiance

The DNs in all bands of the 1G ETM+ imagery Level used in this study are transformed into physical measurements of sensor radiance Conversion of radiance values to sensor brightness temperature (T_B). Eq. (6) was used to transform the spectral radiance to sensor brightness temperature (Wukelic et al., 1989; Landsat Project Science Office, 2002; Chen et al., 2006).

$$T_B = \frac{K_2}{\ln\left(\frac{K1}{L\lambda}\right)+1} - 273 \quad (6)$$

where T_B is the brightness temperature in Celsius (°C), L_λ is the spectral radiance in $Wm^{-2}\ sr^{-1}\ mm^{-1}$; K_2 and K_1 are the prelaunch calibration constants: for Landsat-8: K_1 is 666.09, K_2 is 1282.71 ($W\ m^{-2}\ sr^{-1}\ \mu m^{-1}$).

Emissivity estimation of the land surface from the NDVI

To recover the land surface temperatures, the obtained T_B are scaled based on surface materials emissivity. Emissivity applied to urban surfaces, ranges from 0.87 up to 0.97 (Dousset, 1989; Henry et al., 1989; Balling and Brazel, 1988) with most values in the range 0.92-0.95 (Voogt and Oke, 2003). The emissivity was recovered using (Sobrino et al., 2004; Alsultan et al., 2005 method). A short-term explanation of the method is illustrated as following:

- For NDVI is < 0.2, the pixel is measured as bare land and the mean emissivity value considered in the present study is 0.97. For NDVI values > 0.5, the pixel is totally measured as vegetation, and a constant value for the emissivity (Ɛ) is assumed,

usually of 0.99. For the NDVI values ranging from 0.2 to 0.5, a mixture of the bare land and vegetation composes the pixel, and the emissivity is calculated according to Eqs. (7), (8) and (9) as follows:

$$d\varepsilon = (1 - \varepsilon s)\,(1 - Pv)\,F\,\varepsilon v \quad (7)$$

where, εv and εs are vegetation and soil emissivity, respectively. Pv is the vegetation proportion obtained according to (Sobrino et al., 2004):

$$Pv = \left[\frac{(NDVI-NDVImin)}{(NDVImax-NDVImin)}\right]^2 \quad (8)$$

where F is a shape factor whose mean value, assuming different geometrical distributions, is 0.55 (Sobrino et al., 2004; Alsultan et al., 2005)

$$\varepsilon = \varepsilon v\,Pv + \varepsilon s\,(1- Pv) + d\varepsilon \quad (9)$$

Retrieving the land surface temperature (LST)

Once the emissivity images were obtained, the LST can be derived according to Eq. (10)

$$LST = \frac{TB}{(1+\lambda\sigma\, TB / (hc))} \ln \varepsilon \quad (10)$$

where λ is the effective wavelength (11.475 µm), δ is Boltzmann constant

(1.38 $x10^{-23}$ J/K), h is Plank's constant ($6.626x10^{-34}$ J.S), c is the velocity of light at a vacuum (2.998 $x10^{-8}$ m/sec), ε is emissivity.

Temperatures are classified into proper levels and color-coded to produce a distribution map of the LST over the study area.

Mapping urban heat islands (UHI)

Amorim and Dubreuil (2017) defined the urban heat island intensity as the difference between average temperature of UHI area and that of urban area. This method is also used to measure the intensity of UHI in the study area using Eq. (11 and 12) for each multi-temporal LANDSAT images

$$LST > (\mu + 0.5\ x\ \sigma) \text{ referred to UHI area} \quad (11)$$

$$0 < LST \leq (\mu + 0.5x\sigma) \text{ denoted as non-UHI} \quad (12)$$

where, μ is the mean and σ is the standard deviation of temperatures in Qalyubia Governorate.

Eqs. (11 and 12) were used to categorize the land surface temperature LST images and to represent the spatial distribution of the UHI zones.

Particulate matter (PM10) mapping and assessment

The multispectral bands of the calibrated Landsat OLI image were further processed to map the spatial distribution of PM_{10} in the study area and to assess its levels in UHIs regions. This will be used in integration with the land characteristics to assess the environmental conditions associated with UHIs.

In this study, the multispectral PM_{10} algorithm model for Landsat has been used according to Eq. (13) (Nadzri et al., 2010):

$$PM_{10} = 396\ R_{\lambda 1} + 253\ R_{\lambda 2} - 194\ R_{\lambda 3} \quad (13)$$

where PM_{10} concentration is in ($\mu g/m^3$), $R_{\lambda 1}$, $R_{\lambda 2}$ and $R_{\lambda 3}$ are equal to the atmospheric reflectance of blue, green and red bands, respectively.

Statistical analysis

In this study, a correlation coefficient was calculated between LULC, LST, spectral retrieved indices and PM_{10} using IBM SPSS Statistics 19 software to assess the relationships between these parameters. This helps in finding the main reasons and processes accelerating the formation of UHIs regions. For this, 300 random points were generated using ArcGIS 10.1 and the corresponding values at these points were extracted.

The correlation coefficient is a test to assess the degree to which the measured variables (e.g. x and y) vary together. The correlation coefficient is scaled so that its value is independent of the units in which the two measured variables (x and y) are expressed. The value of any correlation coefficient is between −1.0 and +1.0 (Ramadan, 2003).

Results and Discussions

Environmental characteristics of the study area

As shown in Figs. (2 and 5); LULC and NDVI map showed that the most dominant class in the study area is the agricultural lands (806.85 km^2; 64.45%) which are distributed in the whole area except the eastern part. The eastern part of the study area represents the desert extension of the governorate which is a pioneering area for urban development and reclamation projects. However, the old agricultural lands dominated all the study area where a dense vegetation (NDVI>0.5) is located except the reclaimed land in the desert extension (NDVI 0.25-0.5). This part is classified as a "bare land" which attains a total area of

104.89 km^2, representing 8.38 % of the total area. New urban cities are located in this region (e.g. El-Obour City). Such cities as well as villages and industries are classified as urban area which is scattered in the whole study area. This class represents the second dominant class in the study area (25.79 %, 322.95 km^2). The NDBI was greater than 0.3 as shown in Fig. 6.

The class of "Water bodies" occupied 1.38 % (17.28 km^2) represented by Nile River, irrigation, drainage networks and Arab El-Olikat lakes as shown in LULC and MNDWI maps (figs. 2 and 7) where water bodies recorded MNDWI greater than 0.7. Water bodies and agricultural lands recorded high levels of moisture (NDMI>0.7) as shown in Fig. 8.

The NDSI showed sabkha land in the south eastern part of the study area around Arab El-Olikat lakes which did not appear in the LULC map as shown in Fig. 9.

On the other hand, the study area is well served by road networks as shown in Fig. 3. The main roads network occupied a total length of 936.07 km. The Main irrigation and drainage networks are usually inseparable and mainly associated with the old agricultural lands as shown in Fig. 4. The canal from 5 to 10 m width was the main dominant type in the study area representing 162.12 km length, while a drain from 10 to 25 m width was the dominant type representing 114.96 km length. Second dominant type was canals more than 25 m width occupying lengths of 130.73 km, while second dominant type of drains was from 5 to 10 m width representing 110.76 km length. The least dominant classes were represented by canals from 10 to 25 m width occupying 119.24 km length and drains more than 25 m width occupying lengths of 18.76 km.

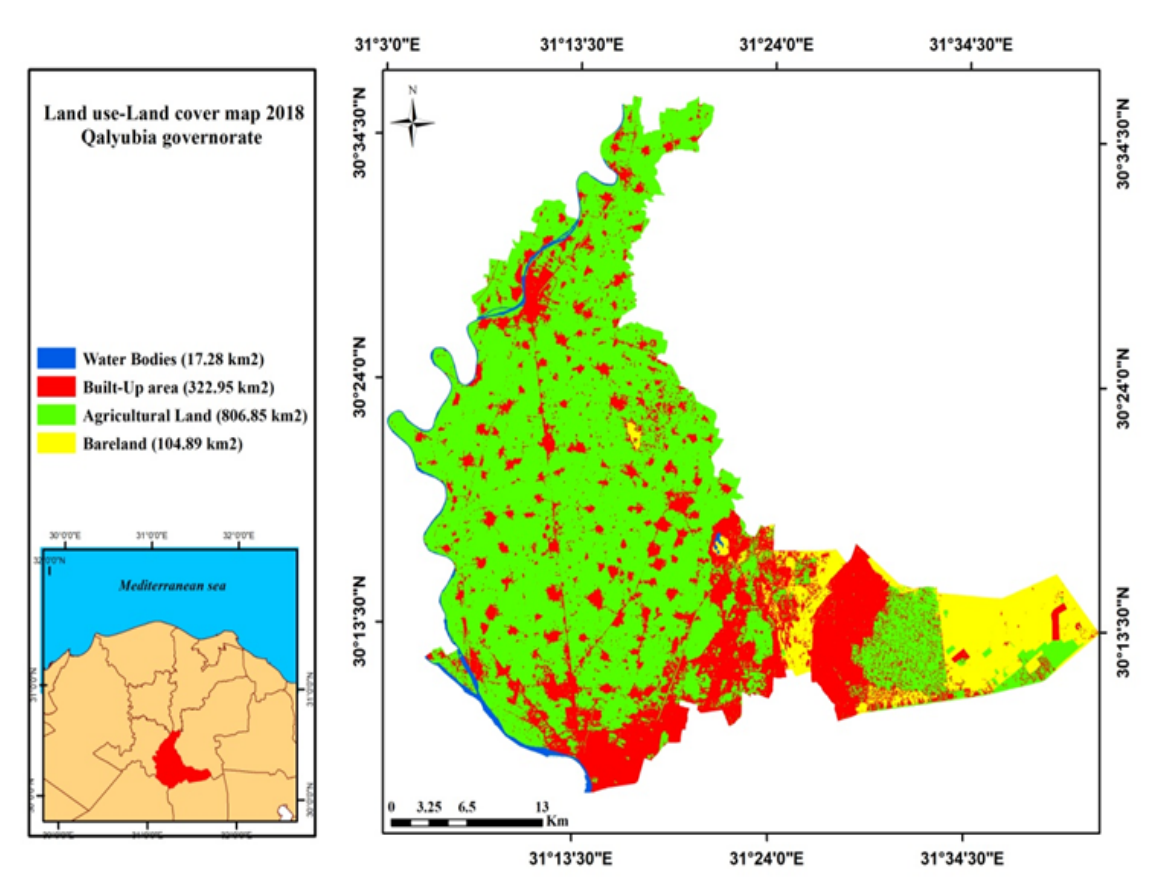

Fig. 2. Map of LULC retrieved from the supervised classification

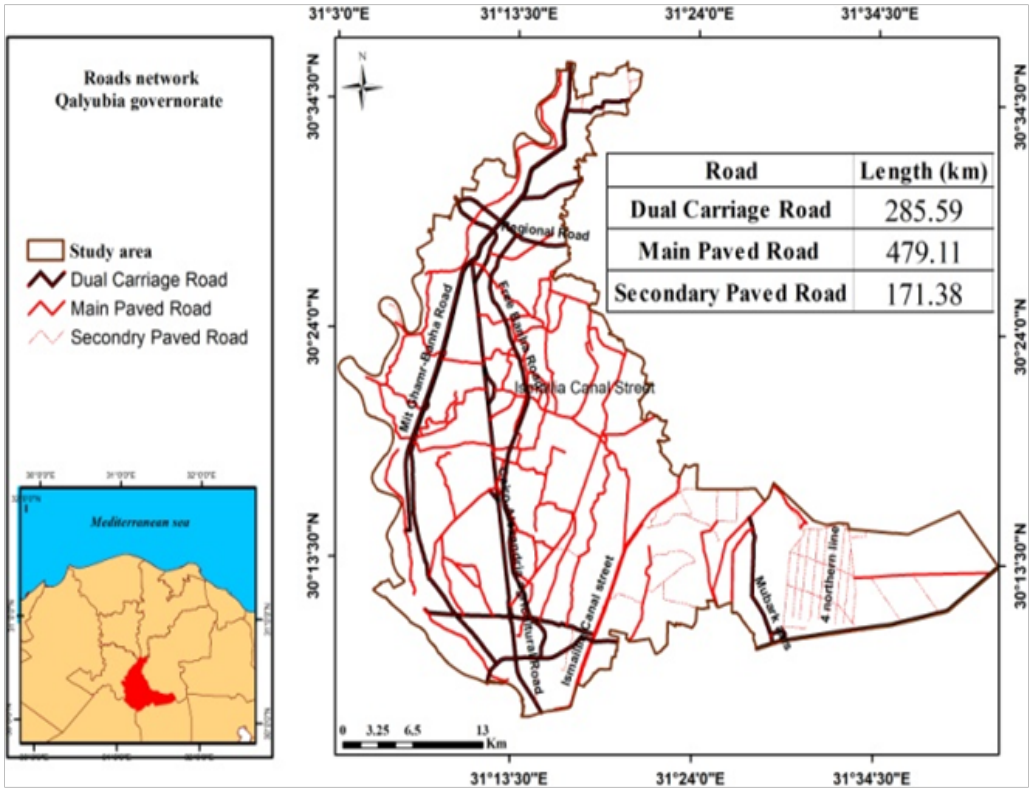

Fig. 3. Roads network in the study area

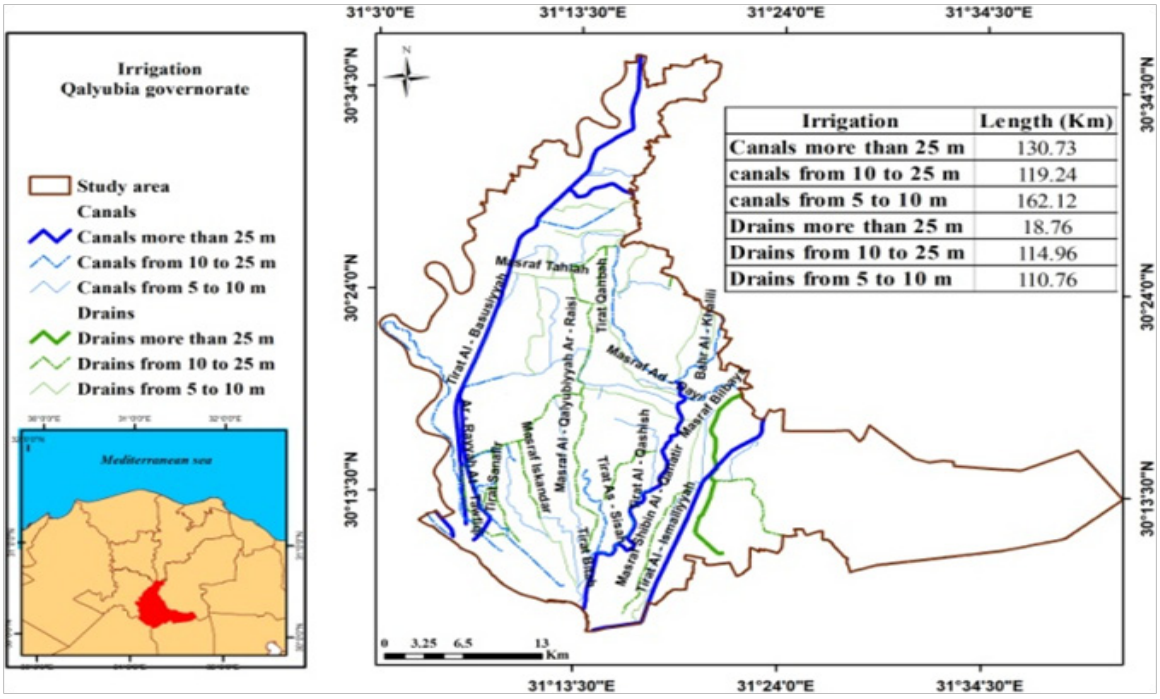

Fig. 4. Irrigation and drainage network in the study area

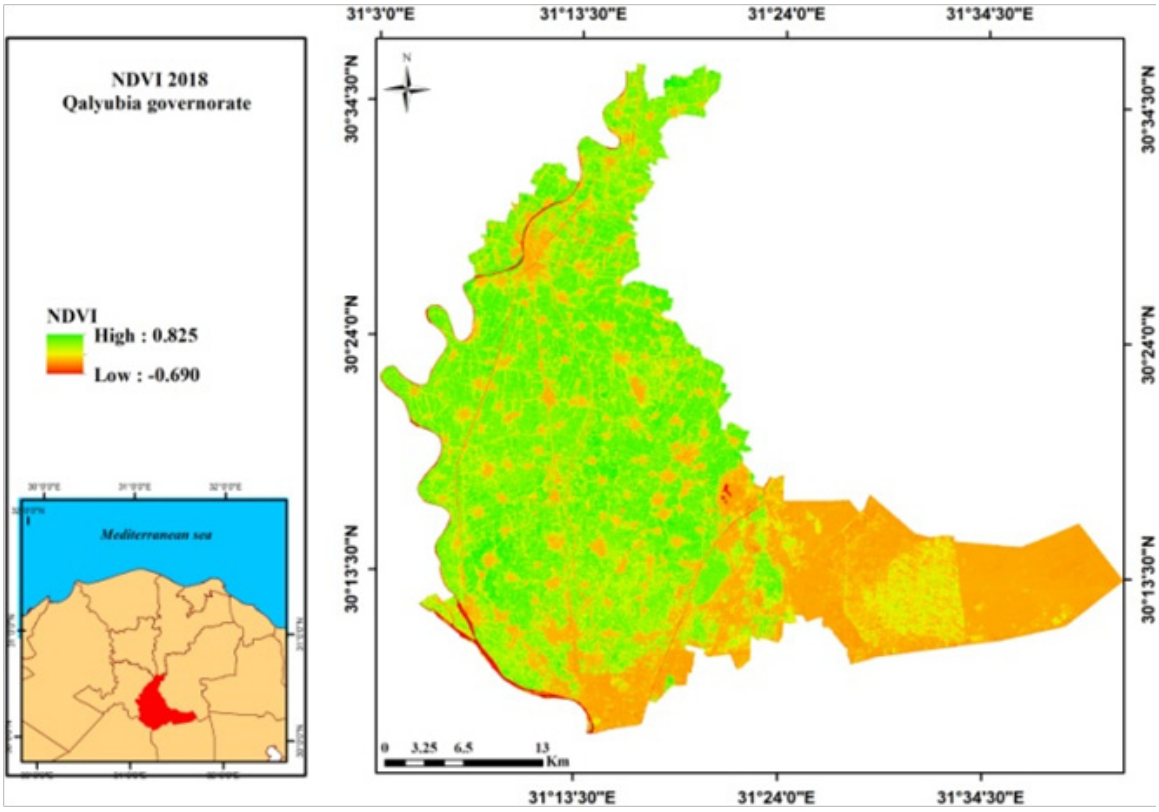

Fig. 5. Map of NDVI in the study area

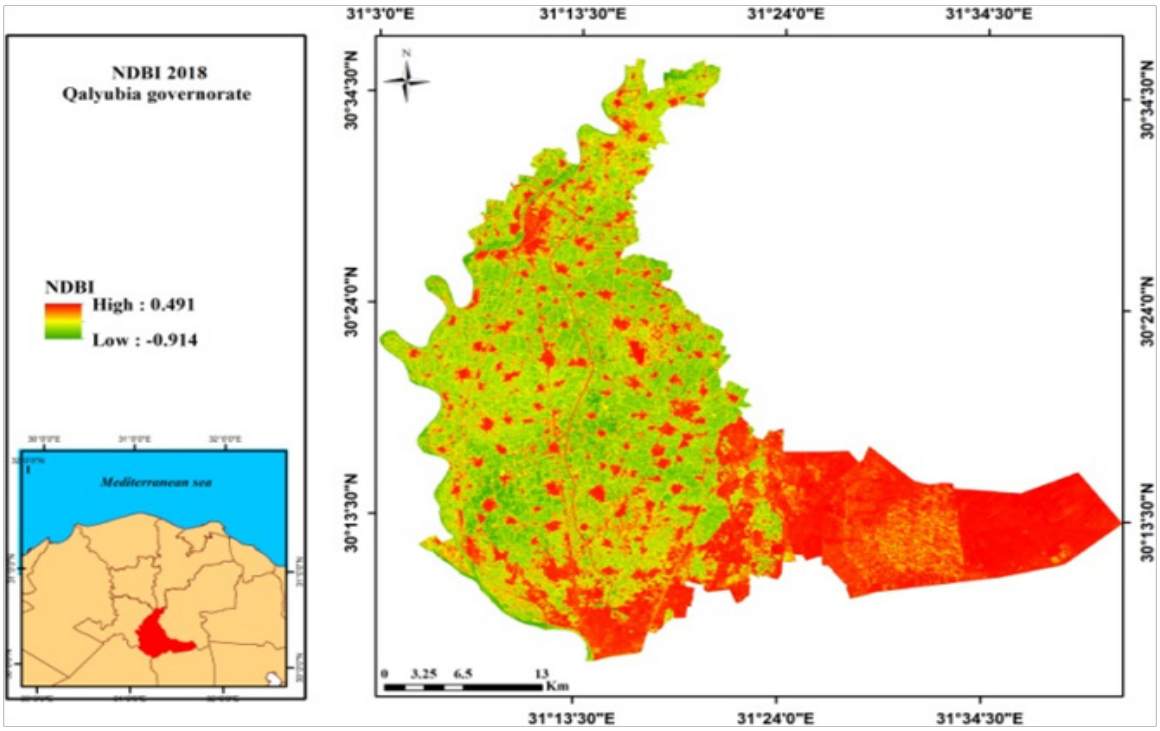

Fig. 6. Map of NDBI in the study area

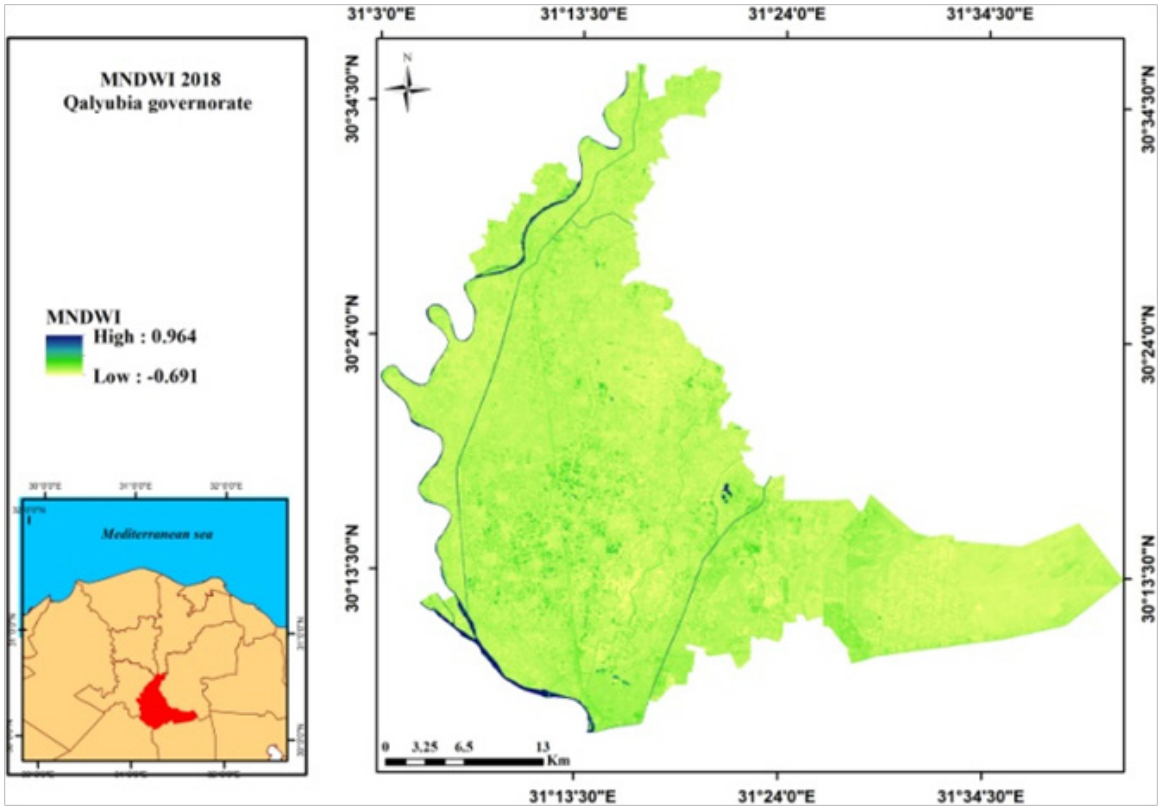

Fig. 7. Map of MNDWI in the study area

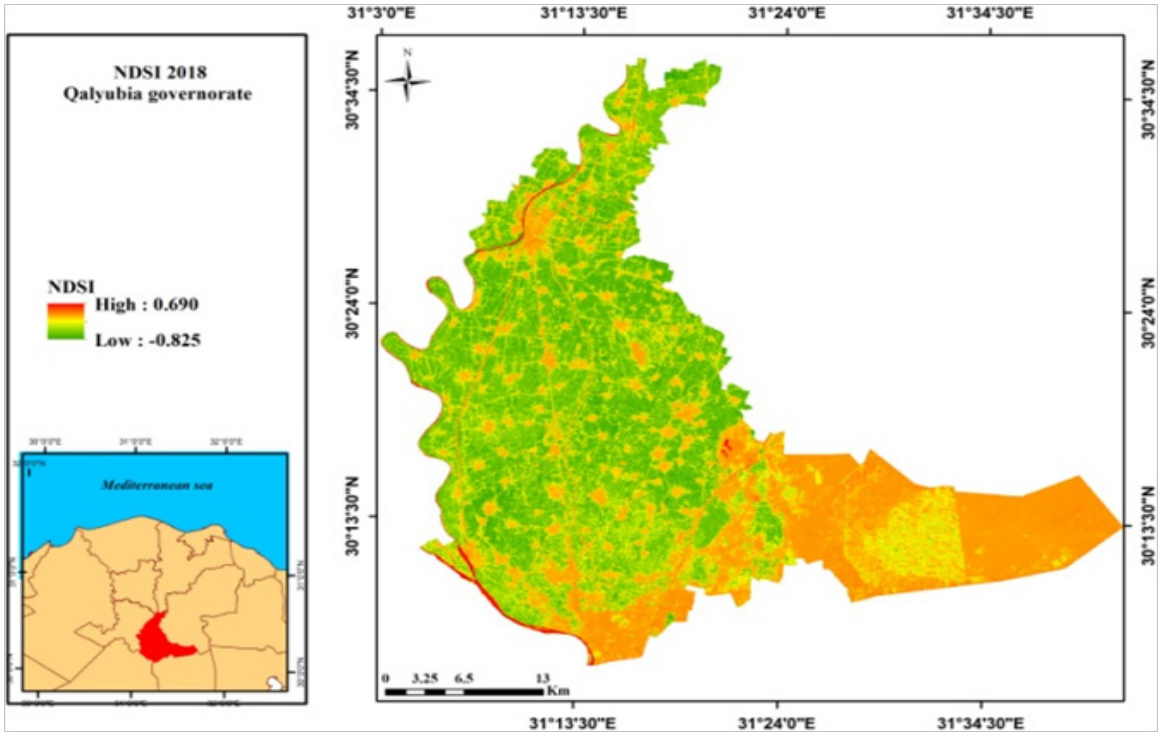

Fig. 8. Map of NDMI map in the study area

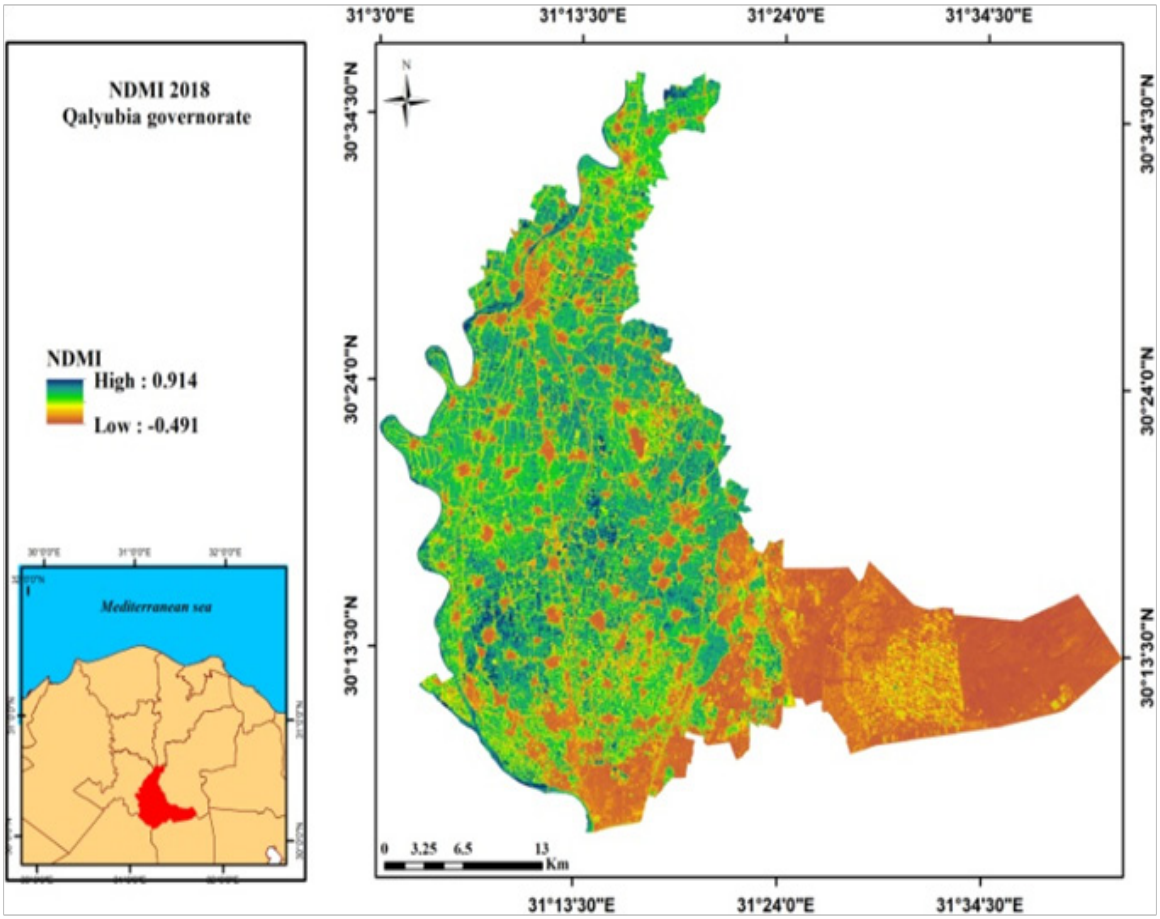

Fig. 9. Map of NDSI in the study area

Land Surface Temperature (LST) and Particulate Matter (PM10)

Spatial variations of LST in the whole governorate are illustrated in Figure 10. Mean LST of each LULC class in Qalyubia Governorate followed this order; bare lands (42°C) > urban (37.9°C) > vegetation (33.02°C) > water bodies (29.2°C) which agrees with El-Zeiny and Effat (2017) who recorded the same arrangements (47.62 °C for bare land, 41.73 °C for urbanized areas, 39.12 °C for vegetation and 33.41 °C for water bodies).

Fig. 10 shows that the highest LST exists not only over the built-up area, but rather it was abundant over the desert (bare land) areas despite the higher albedo in desert. This is confirmed by the significant positive correlation between LST and NDBI (0.843) as shown in Table 1. This is attributed to the lack of both vegetation and water bodies in the desert. This fact is illustrated through the significant negative correlation between LST with NDVI and NDMI (-776 and -0.843), respectively.

Particulate matter (PM10) and its distribution

The spatial distribution map of PM_{10} in the whole study area is illustrated in Fig.11. A great fluctuation in PM_{10} levels is observed since it ranged from 13.6 to 231 µg/m^3 with an average of 81.07 µg/m^3. This fluctuation is mainly attributed to the severity of activities and to the type of land use in the study area. The PM_{10} is basically generated from a variety of human (anthropogenic) activities. These types of activities include agricultural processes, industrial operations, wood and fossil fuels combustion, construction activities, and volatilization of road dust into the air. In the study area, the main anthropogenic sources of PM_{10} are industrial, urban and agricultural activities.

The main dominant industries in the study area are electrical, plastic, automotive, petroleum refining and manufacturing of food and industrial minerals as well as the industrial area of AboZaebal city, which is famous by the industry of fertilizers and chemicals.

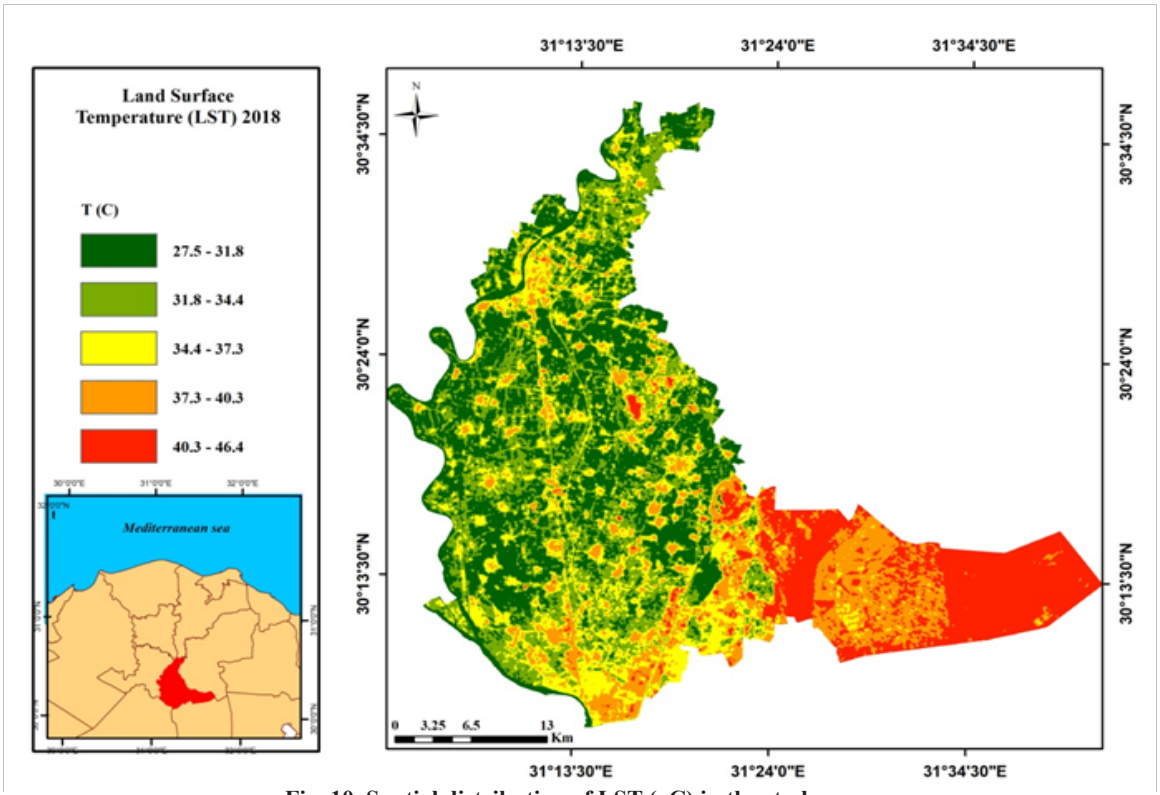

Fig. 10. Spatial distribution of LST (oC) in the study area

TABLE 1. Correlation coefficient between studied parameters.

Parameters	LST	PM_{10}	NDVI	NDBI	NDMI	MNDWI	NDSI
LST	1						
PM_{10}	.318**	1					
NDVI	-.776**	-.016	1				
NDBI	.843**	.105*	-.896**	1			
NDMI	-.843**	-.105*	.896**	-1.000**	1		
MNDWI	-.240**	-.304**	-.184**	-.260**	.260**	1	
NDSI	.776**	.016	-1.000**	.896**	-.896**	.184**	1

**Correlation is significant at the 0.01 level (1-tailed)
* Correlation is significant at the 0.05 level (1-tailed)

In regard of the agricultural area characteristics and activities, the old lands dominate northern parts of the governorate using the flooding irrigation in most parts. The main summer and winter crops in the study area are maize, wheat, rice, corn, clover and some kind of vegetables such as potatoes, tomatoes, cucumbers and carrots. This depends on the availability of water resources and the instructions set by the Egyptian ministry of agriculture to sustain the available resources and ensure the maximum economic income.

Therefore, some high levels of PM_{10} were observed over the urban and agricultural lands. The impact of natural processes on PM_{10} levels is magnified in the desert areas (bare land) which are mainly due to the effect of windblown dust.

Levels of PM_{10} in the study area were evaluated using the threshold limits identified by the WHO and Egyptian standards. Results show that the PM_{10} levels in different districts exceed the allowable limits of WHO air quality standards (50 µg/m^3 as maximum 24-h mean) and the Egyptian standards as well (70 µg/m^3 as maximum 24-h mean) (Fig. 11 and 12).

The most sensitive districts in Qalyubia Governorate are Obour, Khanka and Khosos districts. These districts are in the vicinity to industrial and bare land areas; therefore they are more vulnerable to upper and lower respiratory diseases than the remote districts.

Mapping and characterizing UHIs

The spatial distribution of UHIs in the whole governorate is illustrated in Figure 13. It showed that the hot spots (areas recording high levels of LST) are distributed in the whole governorate area and are mainly associated with the following regions:-

- Built-up areas surrounded by bare lands as shown in El-Obour city in the eastern part of the study area.
- Dense residential areas as shown in Shubra district at the south and in Banha district at north of the study area.
- Built-up areas adjacent to industrial activities as found in Khanka district at the southern east of the governorate.
- Sand covered areas (bare lands) particularly east of the study area.

Land uses associated with the UHIs were mapped in Fig. 14. It is found that most of bare lands and built-up areas exist as heat island patterns. Urbanization is one of the significant factors affecting UHIs, since the urban index showed a strong positive correlation with surface temperature (0.843) as shown in table (1). The total area covered by UHI is 397.5 km^2; 321 km^2 of this area is located in bare land (119.8 km^2, 30.2%) and built-up areas (201.2 km^2, 50.6%) while a small area covered by water (0.2 km^2) and vegetation (76.3 km^2) which are extensively surrounded by urban and industrial areas.

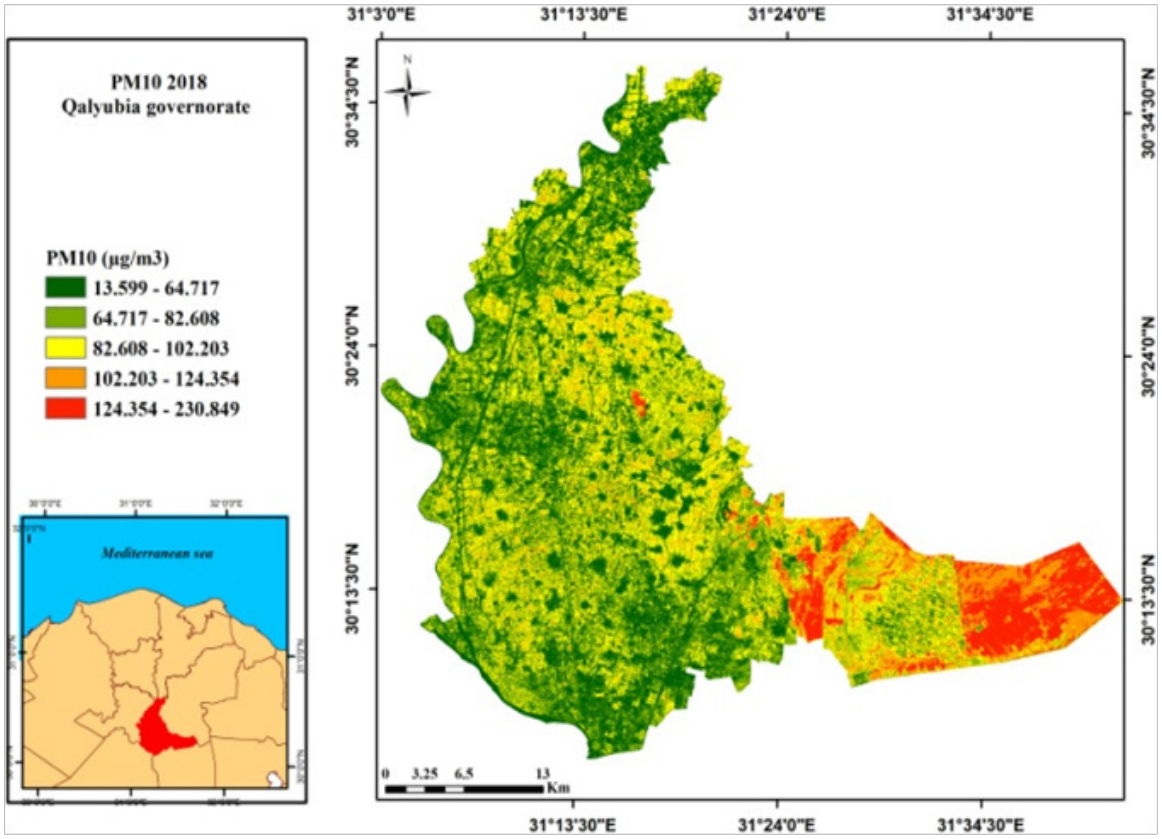

Fig. 11. Spatial distribution of PM10 in the study area

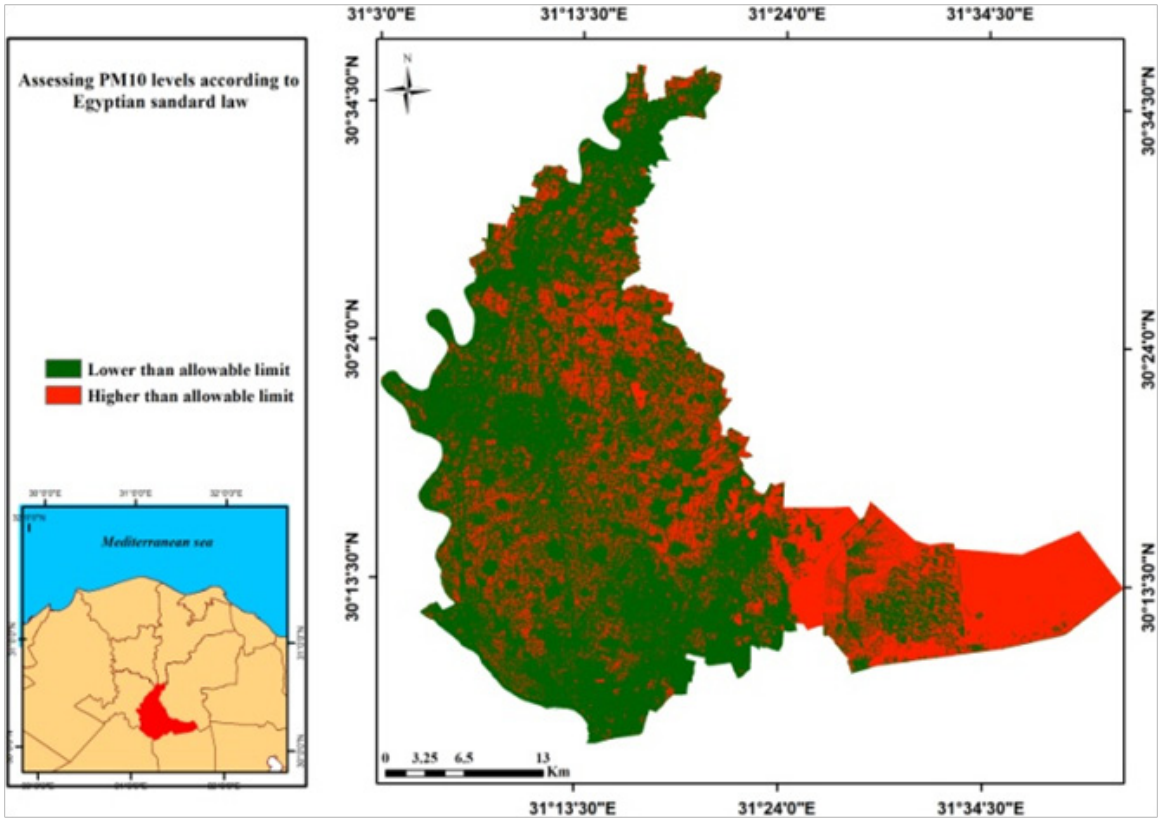

Fig. 12. Assessment of PM10levels according to the Egyptian guidelines

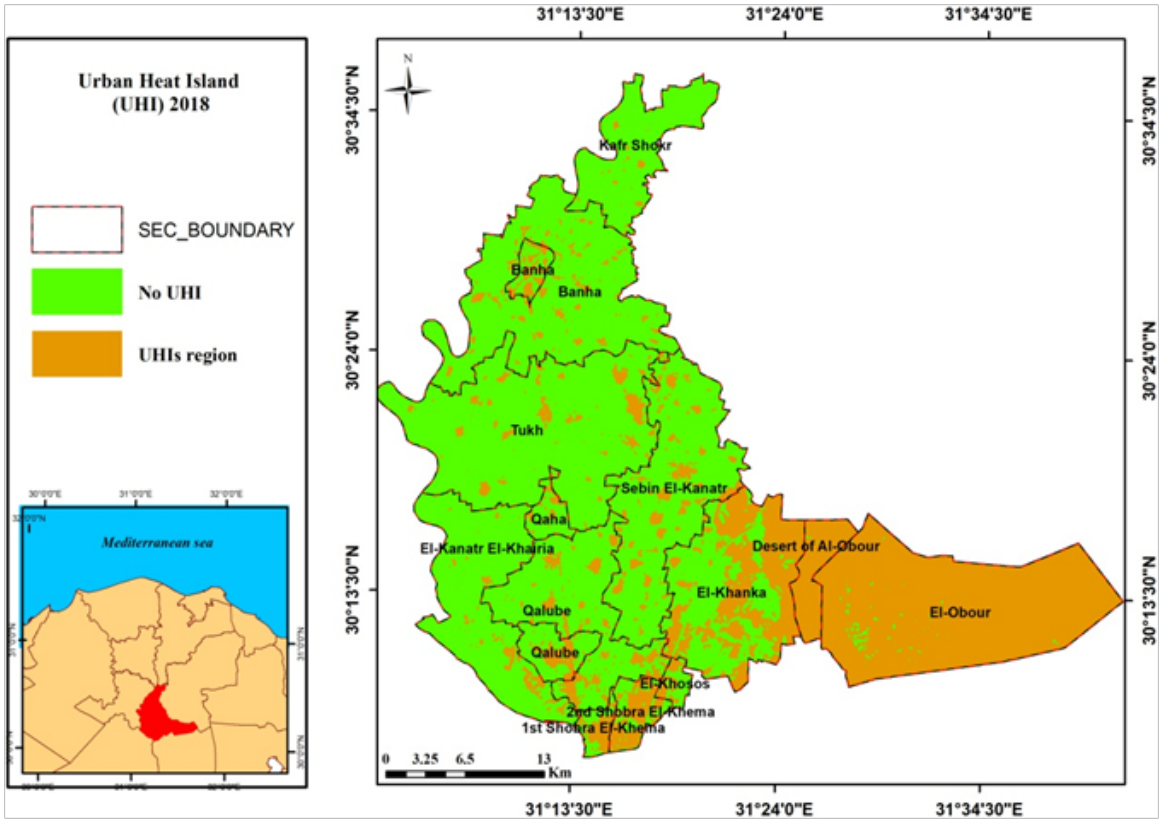

Fig. 13. Spatial distribution of UHIs in the study area

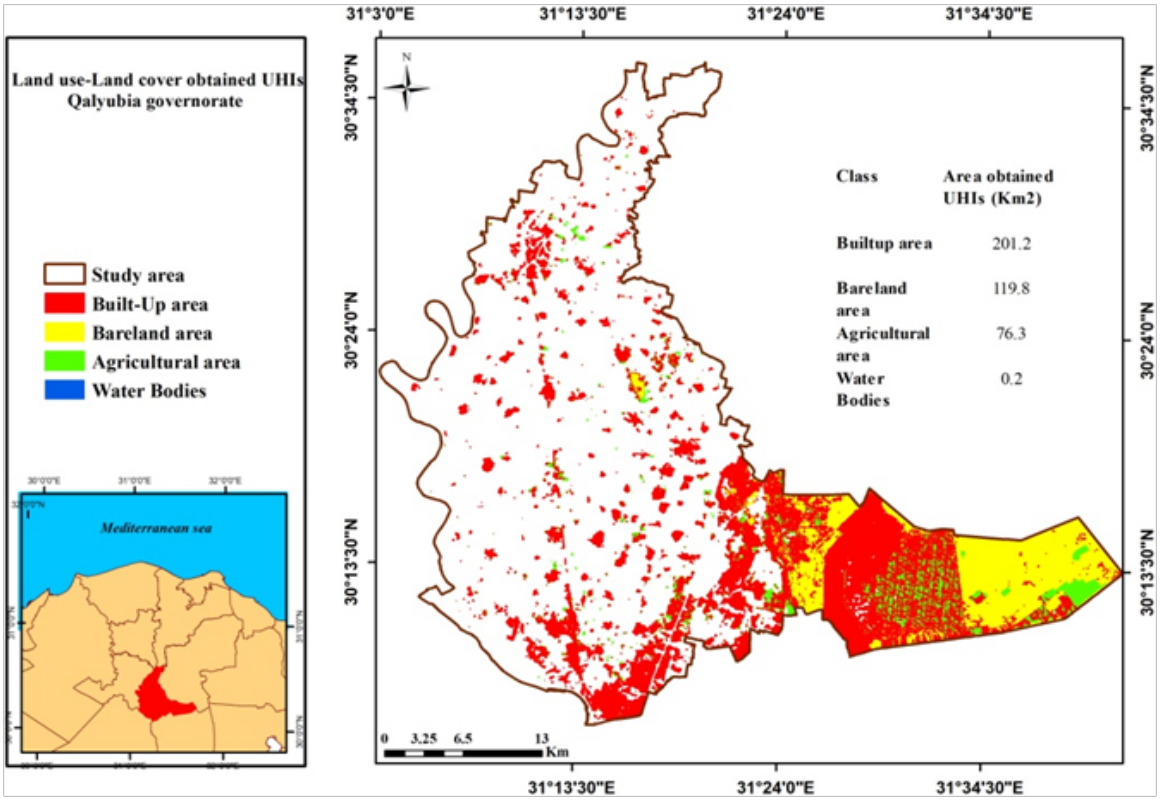

Fig . 14. Different LULC obtained in UHIs regions

Some scattered hotspots exist over built-up and are more abundant in the eastern parts of the city close to desert lands. The hot spot areas (areas with maximum LST) are dispersed in the desert bare lands and in different parts at the city. These regions are those of land-uses related to impermeable cover such as asphalt bus parking, large warehouse, and roads (Effat and Hassan, 2014).

Increase in density, reduction in open spaces and green cover, increase in built-up spaces are proved to increase the heat island phenomenon. These thermal changes deteriorate the urban environment, -causing health problems. Therefore, Urban planners, designers, architects need to consider the urban climate while designing and planning cities.

By comparing average values of NDVI and MNDWI in the study area and in the UHIs regions, it is clear that they decrease in the UHIs regions as shown in Table 2. This result proved that presence of green cover and water bodies decreases heat islands area. On the other hand, average value of NDBI in UHIs regions increase in compared with study area due to reduction in open spaces and green cover.

Moreover, the average value of PM_{10} over UHI (94.26 µg/m^3) is higher than that of the whole study area (81.07 µg/m^3) as shown in Figure 15. This means that air quality is more deteriorated over UHIs than other areas. This is attributed to number of common factors which influence both PM_{10} levels and UHIs thickness. For instance, the industrial activities release more particles to the air which increase the levels of PM_{10}. On the other hand, these activities particularly the heavy industries release more temperature to the environment which consequently has thermal impacts on the surrounding land uses.

Sand covered areas (*i.e.* deserts) can impact the levels of PM_{10} in the air as a result of the wind action which moves the ground sand into the atmosphere. Further, the high reflection power of sand increases the probability of UHIs formation in these regions. Therefore, some areas in the desert might be located in the UHI regions and also record high levels of PM_{10}. The impacts of such factors, which are naturally occurred, are well represented in the eastern part while the anthropogenic factors are magnified in other parts in Qalyubia Governorate particularly within urban areas.

TABLE 2. Statistics of spectral indices and PM_{10} distribution in the whole study area and in UHIs

Parameters	Study area			UHI		
	Min.	Max.	Avg.	Min.	Max.	Avg.
NDVI	-0.7	0.8	0.4	-0.2	0.7	0.16
NDBI	-1	0.5	-0.14	-0.5	0.5	0.03
MNDWI	-0.7	1	-0.2	-0.7	0.5	-0.3
NDMI	-0.5	1	0.14	-0.5	0.5	-0.03
NDSI	-0.8	0.7	-0.4	-0.8	0.2	-0.1
PM_{10} (µg/m^3)	13.6	230.85	81.07	13.6	230.85	94.26

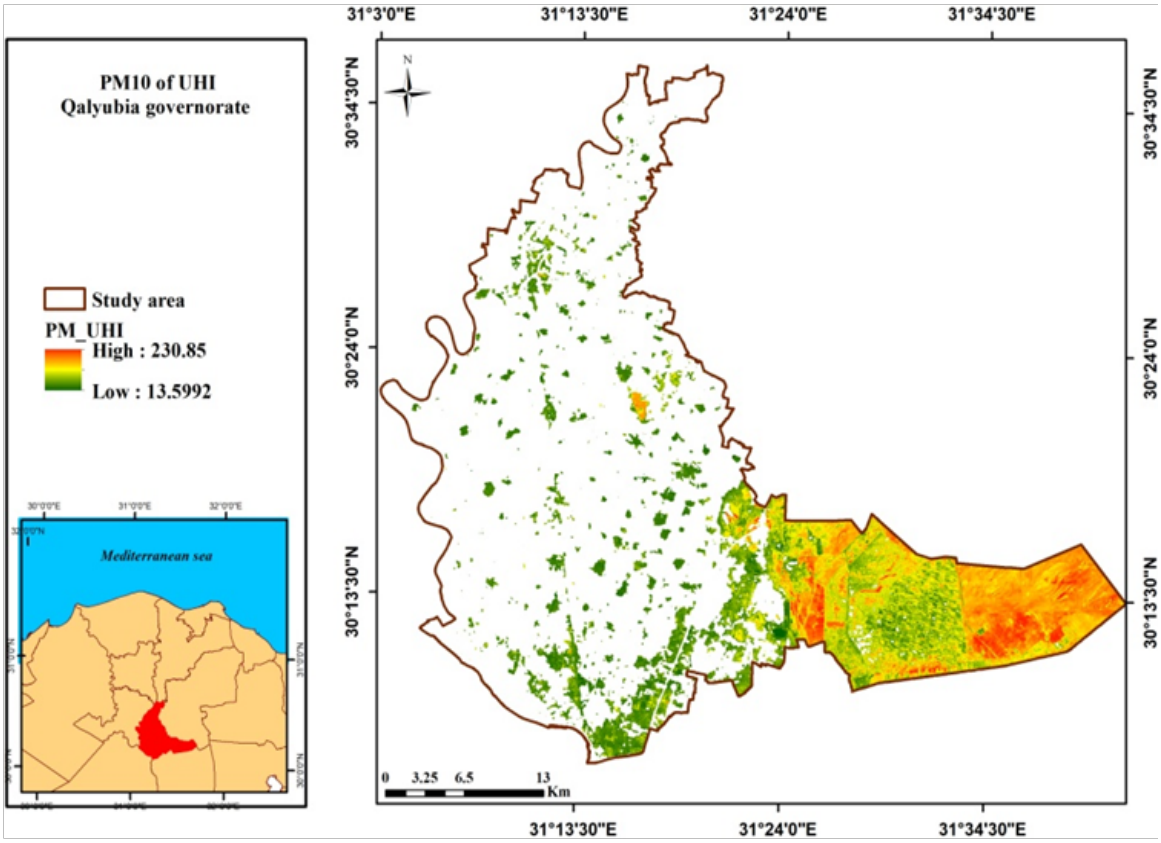

Fig. 15. ThePM10 obtained in UHIs regions

Conclusion

The UHIs are mostly associated with the districts containing residential areas in vicinity to industrial zones and bare lands. The analyses of land use spectral indices and LST showed that the anthropogenic activities viz. urbanization and industrialization impacted not only the thermal characteristics but also the quality of the environment. The zones of UHIs are more deteriorated in regard of air quality, i.e. PM_{10} than other areas which exceeded the Egyptian allowable limits of air quality. Some of these regions are located within the sand covered zones in the desert extension of the governorate. These regions showed high levels of PM_{10} as a result of the wind action. This increased the potentiality of respiratory tract diseases in these areas. On the other hand, it is highly recommended that urban planners, designers and architects should consider thermal characteristics of urban areas during designing and planning cities.

References

Abdel-Hamid H. (2010) Inventory of soil salinity, alkalinity and water logging problems in the Nile Delta, Egypt. *M.Sc. Thesis.* Damietta, Fac. of Science. Mans. Univ.

Ahl D. E., Gower S. T., Burrows S. N., Shabanov N. V., Myneni R. B., and Knyazikhin Y. (2006) Monitoring spring canopy phenology of a deciduous broadleaf forest using MODIS. *Remote Sens. Environ.* **104**, 88-95.

Alsultan S., Lim H. S., Matjafri M. Z. and Abdullah K., (2005) An algorithm for land surface temperature analysis of remote sensing image coverage over Al Qassim, Saudi Arabia. In: From Pharaohs to Geo informatics FIG Working Week 2005 and GSDI-8 Cairo, Egypt April 16-21, 2005. Cited in 30 June 2014 at: https://www.fig.net/pub/cairo/papers/ts_27/ ts27_09_alsultan_etal.pdf.

Amorim M. C. T. and Dubreuil V., (2017) Intensity of Urban Heat Islands in Tropical and Temperate Climates. *Climate* 5, 91; doi:10.3390/cli5040091.

Anim D. O., Kabo-Bah A. T., Nkrumah P. N. and Murava R.T., (2013) Evaluation of NDVI using SPOT-5 satellite data for northern ghana. *Environ. Manage. Sustainable Dev*. **2**, 167-182.

Arya S. P., (2001) Introduction to micrometeorology., International Geophysics Series Academic Press: San Diego, CA. **79** (2).

Arveti N., Etikala B. and Dash P. (2016) Land use/land cover analysis based on various comprehensive geospatial data sets: a case study from Tirupati Area, South India. Adv. Remote Sens. **5** (2), 73-82. http://dx.doi.org/10.4236/ars.2016.52006.

Balling R. C. and Brazel S. W., (1988) High-resolution surface-temperature patterns in a complex urban terrain. Photogr. Eng. Remote Sens. **54**, 1289-1293.

Chen Z., Hu C., and Muller-karger F., (2006)Monitoring turbidity in Tampa Bay using MODIS/Aqua 250-m Imagery, Remote Sens. of Environ. **109**, 207-220.

Cohan A., Donald D. and Wu J., (2011) High resolution pollutant transport in the San Pedro Bay of California. *Atmospheric Pollution Research.* **2**, 237-246.

Coll C., Galve J. M., Shnchez J. M. and Caselles V., (2010) Validation of Landsat-7/ETM+ thermal-band calibration and atmospheric correction with ground-based measurements. IEEE Trans. *Geosci. Remote Sens*. **48**(1), 547-555.

De Boer M. E., (2000) Land cover monitoring: an approach towards pan European land covers classification and change detection. Scientific report. Delft, Beleids Commissie Remote Sensing (BCRS).

Dousset B., (1989) AVHRR-derived cloudiness and surface temperature patterns over the Los Angeles area and their relationship to land use. In: Proceedings of IGARSS-89, IEEE, New York, 2132-2137.

Effat H. and Hassan O., (2014) Change detection of urban heat islands and some related parameters using multi-temporal Landsat images; a case study for Cairo city, *Egypt Urban Clim.* **10**, 171-188.

Elbeih S. F. and El-Zeiny A. M., (2018) Qualitative assessment of groundwater quality based on land use spectral retrieved indices: Case study Sohag Governorate, Egypt. *Remote sens. App*.: Soc. Env., **10**, 82-92.

El-Zeiny A. M. and Effat H. A., (2017)Environmental monitoring of spatiotemporal change in land use/land cover and its impact on land surface temperature in El-Fayoum governorate, Egypt. Remote sensing applications: society and environment.

El-Zeiny A. and El-Kafrawy S. (2017) Assessment of water pollution induced by human activities in Burullus Lake using Landsat 8 operational land imager and GIS. *The Egyptian Journal of Remote Sensing and Space Sciences*; **20**, S49-S56.

Gao B. C. (1996) A normalized difference water index for remote sensing of vegetation liquid water from space. *Remote Sensing of Environment* **58**, 257-266.

Hajat S., O'Connor M. and Kosatsky T., (2010)Health effects of hot weather: from awareness of risk factors to effective health protection. *The Lancet* **375**, 856– 863.

Henry J. A., Dicks S. E., Wetterqvist O. F. and Roguski S. J., (1989) Comparison of satellite, ground-based, and modeling techniques for analyzing the urban heat island. *Photogr. Eng. Remote Sens*. **55**, 69-76.

Huang S., and Siegert F., (2006) Land cover classification optimized to detect areas at risk of desertification in North China based on SPOT VEGETATION imagery. *J. of Arid Environ.t.* **67**, 308-327.

Jabbar M. and Xiaoling C., (2008) Land degradation due to salinization in arid and semi-arid regions with the arid of geo-information techniques. *Geo. Spat. Inform. Sci.* **11**(2), 112-120.

Jay O. and Kenny G. P., (2010) Heat exposure in the Canadian workplace. *Am. J. Ind. Med.* **53**, 842-853.

Ji L., Zhang L. and Wylie B., (2009) Analysis of dynamic thresholds for the normalized difference water index. *Photogramm. Eng. Remote Sens*. **75**, 1307-1317.

Jones P. D., Wigley T. M. L. and Wright P. B., (1986) Global temperature variations between 1861 and 1984. *Nature,* **332**, 430-434.

Kleerekoper L., van Esch M. and Salcedo T. B., (2012) How to make a city climate-proof, addressing the urban heat island effect. *Resour. Conserv. Recycl.* **64**, 30-38.

Landsat Project Science Office, (2002) *Landsat 7 Science Data User's Handbook.* Goddard Space Flight Center, NASA, Washington, DC, cited from: http://ltpwww.gsfc.nasa.gov/IAS/handbook/handbook_toc.html.

Liping C., Yujun S. and Saeed S. (2018) Monitoring and predicting land use and land cover changes using remote sensing and GIS techniques —A case study of a hilly area, Jiangle, China. PLoS ONE, **13** (7), e0200493.https://doi.org/10.1371/ journal. pone.0200493.

Lo C. and Shipman R. L. (1990) A GIS approach to land-use change dynamics detection. Photogramm. *Eng. Remote Sens*. **56** (11), 1483-1491.

Masek J. G., Lindsay F. E. and Goward S. N., (2000) Dynamics of urban growth in the Washington DC metropolitan area, 1973–1996, from Landsat observations, *Int. J. Remote Sens*., **21** (18), 3473-3486.

McFeeters S., (1996) The use of Normalized Difference Water Index (NDWI) in the delineation of open water features. *Int. J. Remote Sens.* **17**, 1425-1432.

Nadzri O., Mohd Z. M. J. and Lim H. S., (2010) Estimating particulate matter concentration over arid region using satellite remote sensing: A Case Study in Makkah, *Saudi Arabia. Mod. app. Sci.* **4**, 131-142.

Nakayama T. and Hashimoto S., (2011) Analysis of the ability of water resources to reduce the urban heat island in the Tokyo megalopolis. *Environ. Pollut.* **159**, 2164-2173.

Ramadan A., (2003) Heavy metal pollution and biomonitoring plants in Lake Manzala, Egypt. *Pak. J. Biol. Sci.* **6** (13), 1108-1117.

Rao P. K., (1972) Remote sensing of urban heat islands from an environmental satellite. *Bull. Am. Meteorol. Soc.* **53**, 647-648.

Santamouris M., Papanikolaou N., Livada I., Koronakis I., Georgakis C., Argiriou A. and Assimakopoulos D. N. (2001) On the impact of urban climate to the energy consumption of buildings. *Solar Energy,* **70,** 201-216. http://dx.doi.org/10.1016/S0038-092X(00)00095-5

Shalaby A. and Moghanm F. S., (2015) Assessment of urban sprawl on agricultural soil of northern Nile Delta of Egypt using RS and GIS. *Chin. Geog. Sci.* **25** (3), 274-282.

Shalaby A. and Tateishi R., (2007) Remote sensing and GIS for mapping and monitoring land cover and land-use changes in the Northwestern coastal zone of Egypt, *Applied Geography*, **27**(1), 28–41.

Shen P., Zhang J. and Su Z., (2011) The application of remote sensing in the extraction of urban land-use changes. *Procedia Environ. Sci.* **10**, 1589-1594.

Sobrino J. A., Jimenez-Munoz J. C. and Paolini L., (2004) Land surface temperature retrieval from Landsat TM5, remote sensing of the environment 9, 434-440. ftp://atmosfera.cl/pub/elias/Paula/2004_Sobrino_RSE.pdf.

Teka H., Madakadze C. I., BotaiJ. O., Hassen A., Ayana, Angassa, and Mesfin Y. (2018) Evaluation of land use land cover changes using remote sensing Landsat images and pastoralists' perceptions on range cover changes in Borana rangelands, Southern Ethiopia. *Int. J. Biodiv. Conserv.* **10** (1),1-11.

Tomlinson C. J., Chapman L., Thornes J. E. and Baker C. J., (2012) Derivation of Birmingham's summer surface urban heat island from MODIS satellite images. *Int. J. Climatol.* **32**, 214-224.

Tucker C. J., (1979) Red and photographic infrared linear combinations for monitoring vegetation. *Remote Sens. of the Environ*. **8**, 127-150.

Voogt J. A. and Oke T. R., (2003) Thermal remote sensing of urban climates. *Remote Sens. Environ.* **86**, 370-384.

Weigand C. L. and Richardson A. J., (1990) Use of spectral vegetation indices to infer leaf area, evapotranspiration and yield. *J. of Agron.* **82,** 623-629.

Wukelic G. E., Gibbons D. E., Martucci L. M. and Foote H. P., (1989) Radiometric calibration of Landsat Thematic Mapper thermal band. *Remote Sens. Environ.* **28**, 339-347.

Xu H., (2006) Modification of normalized difference water index (NDWI) to enhance open water features in remotely sensed imagery, *Int. J Rem. Sens.* **27,** 3025-3033.

Zha Y., Gao J. and Ni S., (2003) Use of Normalized difference Built-Up Index in automatically mapping urban areas from TM. Imagery. *Int. J. Remote sens.* **24** (3), 583-594.

التوصيف البيئى والمكانى لمناطق الجزر الحرارية بمحافظة القليوبية، مصر

محمود سالم ابراهيم[١] ، مى ابراهيم الجمال[١] ، عادل سالم شلبى[٢] ، أحمد محمد الزينى[٢] ، نيفين جمال رستم[٢]

[١]قسم علوم البيئة - كلية العلوم - جامعة دمياط - دمياط الجديدة - مصر
[٢]شعبة الدراسات البيئية واستخدامات الاراضى - الهيئة القومية للاستشعار عن بعد وعلوم الفضاء - القاهرة - مصر

تمثل الدراسة الحالية المحاولة الأولى والتى تتناول دراسة و تحديد مناطق الجزر الحرارية وتقييم الظروف البيئية المرتبطة بها فى محافظة القليوبية باستخدام الاستشعار من البعد ونظم المعلومات الجغرافية والمسح الميداني. تمت معالجة صورة القمر الصناعى من النوع لاندسات والملتقطة بتاريخ ٢٢ يوليو ٢٠١٨ لحساب درجة حرارة سطح الارض والجزر الحرارية وغطاء واستخدام الارض وتقييم الظروف البيئية من خلال حساب المؤشرات الطيفية. تم دراسة المؤشرات الآتية: مؤشر الغطاء الحضرى، مؤشر الغطاء النباتى، مؤشر المياه المعدل، مؤشر الملوحة ومؤشر الرطوبة. أيضا تم تطبيق نموذج رياضى على المرئيات الفضائية المصححة لاستخراج ورسم خرائط للجسيمات العالقة بالهواء والتى يبلغ قطرها اقل من ١٠ ميكروميتر ولتقييم مستوياتها فى مناطق الجزر الحرارية. اظهرت النتائج أن متوسط درجات الحرارة بمحافظة القليوبية اتبعت الترتيب الأتى: المناطق الصحراوية تليها المناطق الحضرية ثم الاراضى المزروعه واخيرا المسطحات المائية. صنفت معظم الاراضى الصحراوية والمناطق الحضرية كمناطق جزر حرارية و تبلغ المساحة الاجمالية لمناطق الجزر الحرارية ٣٩٧,٥٢ كم^2، منها ٣٠,٢٪ أراضى صحراوية ، ٥٠,٦٪ مناطق حضرية ، ٠,٠٥٪ مسطحات مائية ، ١٩,٢٪ مناطق زراعية. يعمل وجود الغطاء النباتى والمسطحات المائية على الحد من ظاهرة الجزر الحرارية وهذا ماتفسره المستويات المنخفضة لمؤشر الغطاء النباتى ومؤشر الماء فى مناطق الجزر الحرارية. من ناحية اخرى سجلت الدراسة زيادة فى متوسط قيم مؤشر الغطاء الحضرى بمناطق الجزر الحرارية مقارنة بمنطقة الدراسة. أيضا سجلت الدراسة ازدياد متوسط تركيز الجزيئات المعلقة بالهواء بمناطق الجزر الحرارية (٩٤,٢٦ ميكرو جرام /م^3) عنها فى منطقة الدراسة (٨١,٠٧ ميكرو جرام /م^3). يمكن أن نستخلص أن انخفاض مساحة البقعة الخضراء والمسطحات المائية وزيادة الكثافة الحضرية يزيد من فرصة تكون الجزر الحراية. توصى الدراسة بأهمية الأخذ فى الاعتبار مخرجات مثل هذه الدراسة لصناع القرار مثل المخططين الحضريين والمهندسين المعماريين قبل عمل تخطيط معمارى وتصميم للمدن.